INSTITUTE OF PLASMA PHYSICS

NAGOYA UNIVERSITY

High Power ICRF Heating Experiments on the JIPP T-IIU Tokamak

Y. Ogawa, K. Masai, T. Watari, R. Akiyama, R. Ando, J. Fujita, Y. Hamada, S. Hirokura, K. Ida, K. Kadota, E. Kako, O. Kaneko, K. Kawahata, Y. Kawasumi, S. Kitagawa, T. Kuroda, K. Matsuoka, A. Mohri, S. Morita, A. Nishizawa, N. Noda, I. Ogawa, K. Ohkubo, Y. Oka, S. Okajima, T. Ozaki, M. Sasao, K. Sato, K.N. Sato, S. Tanahashi, Y. Taniguchi, K. Toi, H. Yamada

(Received — Mar. 10, 1989)

IPPJ- 903 Mar. 1989

RESEARCH REPORT

NAGOYA, JAPAN

High Power ICRF Heating Experiments on the JIPP T-IIU Tokamak

Y. Ogawa, K. Masai, T. Watari, R. Akiyama, R. Ando, J. Fujita, Y. Hamada, S. Hirokura, K. Ida, K. Kadota, E. Kako[a)], O. Kaneko, K. Kawahata, Y. Kawasumi, S. Kitagawa, T. Kuroda, K. Matsuoka, A. Mohri, S. Morita, A. Nishizawa, N. Noda, I. Ogawa, K. Ohkubo, Y. Oka, S. Okajima*, T. Ozaki, M. Sasao, K. Sato, K.N. Sato, S. Tanahashi, Y. Taniguchi, K. Toi, H. Yamada

Inst. of Plasma Physics, Nagoya Univ., Nagoya 464-01, Japan
*) Dept. of Applied Physics, Chubu Univ., Kasugai 487, Japan

(Received - March 10, 1989)
IPPJ - 903 March 1989

Further communication about this report is to be sent to the Research Information Center, Institute of Plasma Physics, Nagoya University, Nagoya 464-01, Japan.

Abstract

In the JIPP T-IIU tokamak, a high power ICRF heating experiment has been conducted up to an extremely high power density (~ $2MW/m^3$) with a total rf power of P_{rf} = 2 MW. Much attention has been paid initially to the problem of impurities, and it has been found that a) the adoption of low-Z materials for the limiter, b) *in situ* carbon coating (i.e., carbonization) and c) adequate gas-puffing synchronized to the rf pulse are very effective in suppressing radiation loss. In combination with these methods, a remarkable reduction in metal impurities (especially in iron impurity) has been achieved, suppressing the total radiation loss to less than 30 ~ 40% of the input power. In these reduced-radiation-loss plasmas, characteristics of ICRF-heated plasmas have been intensively studied. With an increase in the ICRF heating power, the deterioration of the energy confinement time has been observed, indicating quantitative agreement with Kaye-Goldston L-mode scaling. It is shown that the so-called profile consistency, which is the leading feature in NBI-heated plasmas, holds also in the ICRF-heated plasma. It has been observed that the electron temperature profile responds only to the safety factor q(a), and is not changed by the deposition profile controlled by tailoring the $k_{\parallel}$-spectrum.

I. Introduction

In order to achieve an ignition condition in a tokamak device, auxiliary heating is indispensable, and most prominent candidates for reactor-grade plasmas from the scientific and economical viewpoints are considered to be the Neutral Beam Injection (NBI) and the wave heating with the Ion Cyclotron Range of Frequencies (ICRF). In ICRF heating, there are several different heating scenarios (e.g., minority heating or 2nd/3rd harmonic heating), and there is a choice between high- or low-field-side excitations. The scientific proofs for these different heating schemes have been done in many tokamak devices [1,2]. Since the mechanism of heating by ICRF waves is quite different from that by NBI, ICRF-heated plasmas are expected to reveal new characteristics different from that of NBI-heated ones, and to advance the understanding of the properties of tokamak plasmas. Accordingly, high power ICRF heating experiments have been conducted in PLT [3], JIPP T-IIU [4], JFT-2M [5], ASDEX [6], TEXTOR [7], JET [8] and JT-60 [9].

In ICRF heating experiments, a high power injection is, in general, limited by the problem of impurities. In the JIPP T-IIU tokamak, we have succeeded in suppressing the radiation loss using several techniques in combination, and extended the heating power up to 2 *MW*. Compared with other devices, the volume-averaged heating power density (~ 2 MW/m^3) is significantly larger and is comparable with that of the Compact Ignition Tokamak (CIT) device, where the plasma volume is 9.5 m^3 and the ICRF power is projected to be 20 *MW* [10]. In this article, the principal results of 2 *MW* ICRF heating experiments on the JIPP T-IIU are described. Recently, H-mode discharges have been achieved for ICRF-heated plasmas in the JIPP T-IIU tokamak, but data of the H-mode are not included.

The experimental setup and typical diagnostics are presented in Section II. In Section III, characteristics of high-power ICRF-heated plasmas are described, including the heating efficiencies for electrons and ions, the confinement

property and MHD activity. It is expected that ICRF-heated plasmas will give information useful for understanding the physics of the constraint on electron temperature profile (so-called profile consistency) [11], because the heating schemes of NBI- and ICRF-heated plasmas are quite different. Then, some aspects related to the profile consistency on ICRF-heated plasmas are described in Section IV. To inject an rf power of 2 *MW*, it is necessary to solve the problem of impurities. With the modelling for impurity suppression, experimental results related to the problem of impurities are presented in Section V. Finally, conclusions are given in Section VI.

II. Experimental arrangements and diagnostics

In the JIPP T-IIU tokamak (R/a = 0.91 /0.23 *m*, with a circular cross section and B_T = 3 *T*), high power ICRF heating experiments up to 2 *MW* have been conducted with a mode-conversion heating scheme, where the applied wave frequency is 40 *MHz*, and a deuterium plasma with 10 % hydrogen minority ions is employed. The layout of the device is shown in Fig. 1, indicating the relative position of the antennas, limiters and diagnostics. On the high-field side six loop antennas are installed; each antenna has a capability of injecting rf power up to 0.5 *MW*, and the phase of the rf wave for each antenna can be controlled as desired. The results of the antenna phasing experiments have been reported by R. Ando *et al.* [12], where the improvement of the electron heating efficiency for $\Delta\varphi = \pi$ has been reported and impurity problem has also been discussed.

The vacuum vessel and the Faraday shield of the antenna are made of stainless steel, while all of the limiters (poloidal limiter, upper/lower limiter and inner limiter) are made of carbon. Both sides of the antenna are also protected by the carbon plates, as shown in Fig. 1. The plasma is usually placed so that it touches the poloidal limiters on the high-field side

with a clearance of about 4 *cm* on the low-field side. The front face of the antenna (i.e., the Faraday shield) is located about 1 *cm* behind these limiters. Sometimes, *in situ* carbon coating, called carbonization, has been carried out to reduce radiation loss due to metal impurity contamination. The location of the electrode used for carbonization is also shown in Fig. 1.

The line-averaged density is measured with 2-*mm* and/or FIR(HCN laser; 337 *μm*) interferometers. The electron temperature profile is measured with a 10-channel grating polychromator for Electron Cyclotron Emission (ECE) measurement [13]. The ion temperature has been measured by several methods: with a charge-exchange fast neutral analyzer (FNA) of the E//B mass-separation type, with a crystal spectrometer (*TiXXI* *w* 2.61 Å), with a VUV spectrometer (*FeXXII* 845.5 Å) and with charge-exchange recombination spectroscopy (CXRS: *CVI* 5292 Å) [14]. The radiation loss is measured with bolometers; a metal bolometer is used to measure the total radiation loss and, pyro detectors are employed for the profile measurement of the radiation loss [15]. To observe the behaviors of various impurity ions, spectrometers for VUV and visible wavelength range are used. An poloidal array of magnetic probes is installed inside the vacuum chamber to measure the magnetic fluctuations, and in addition to determine the plasma position and the total stored energy.

III. Characteristics of high power ICRF-heated plasmas

In Fig. 2 the time evolutions of typical plasma parameters are shown, where the rf power is P_{rf} = 2 *MW* and the plasma current is I_P = 280 *kA*. The marked increase in the density is inevitable in the high power heating in the JIPP T-IIU tokamak. It is mainly due to enhanced recycling on the application of rf, and partly due to the gas-puffing synchronized to the rf pulse. As shown in Fig. 3, the line-averaged density increases

proportionally to the rf power with an off-set level, which comes from the gas-puffing (i.e., $\bar{n}_e = 3x10^{19}m^{-3}$ before the rf and $\bar{n}_e = 5x10^{19}m^{-3}$ during the rf if $P_{rf} < 0.2$ *MW*). The increments in the density with increase in rf power can be attributed to the enhancement of particle recycling, since the amount of gas-puffing is not changed at $0 < P_{rf} < 2$ *MW*. In a relatively small machine, where the ratio of the plasma volume to the surface is small, the change of the influx rate from the wall/limiter affects the plasma density remarkably.

The central electron temperature rises to $T_e(0) = 2.5$ *keV* or more in the early phase of the rf pulse ($t \sim 140$ *ms*; "transient" phase). This comes from the direct electron heating by the mode-converted Ion Bernstein Wave(IBW). In the later phase of the rf pulse ($t \sim 180$ *ms*; "steady-state" phase), the electron temperature slightly decreases and settles to a value of around 2.0 *keV*. Meanwhile, the electron density increases gradually during the rf pulse, and therefore, the electron stored energy $W_e(0)=3/2n_e(0)T_e(0)$ increases monotonically with a time constant of 10 ~ 20 *ms*, as shown in Fig. 2. In Fig. 3, the central electron temperatures at two different time ($t \sim 140$ *ms* and $t \sim 180$ *ms*)are presented as a function of the rf power. The electron temperature in the transient phase ($t \sim 140$ *ms*) increases monotonically as the rf power is raised, and that in the steady-state phase($t \sim 180$*ms*) seems tc become saturated around $T_e(0) = 2.0$ *keV*.

The central ion temperature gradually increases from $T_i(0) = 0.5$ *keV* at the ohmic phase to $T_i(0) = 1.7$ *keV* with a time constant of 30 ~ 40 *ms*, as shown in Fig. 2. Figure 3 shows that the ion temperature seems to assume an increasing curve in proportion to the rf power in contrast to the electron temperature, and ion temperatures as measured by the different diagnostics are in good agreement, even though they refer to temperatures of different ion species. The charge-exchange spectrum of the deuterium ions has a Maxwellian distribution, while that of the hydrogen ions has a high energy tail having a

effective tail temperature $T_{eff,H}$ of 4 ~ 7 keV. The heating power density of hydrogen ions has been experimentally estimated to be $P_{rf,H}(0) \sim 1\ MW/m^3$ near the plasma center [16], and the effective temperature of the hydrogen tail experimentally observed is consistent with Stix's theory [17], where with his notations $T_{eff,H} \sim (1+\xi)T_e$, and the parameter ξ ($=P_{rf,H}\tau_s/(3n_H T_e)$, τ_s is a slowing-down time) is around 2 ~ 3.

The partition of the rf power to each species has been analyzed with a global wave code [18], where one-dimensional slab geometry has been employed with 10 % H-minority plasmas. Calculational results show that the ICRF wave excited by the high-field-side antenna is mainly converted to an Ion Bernstein wave and absorbed by electrons. The percentage of the rf power delivered to electrons is estimated to be 60 ~ 80 %, and that to hydrogen ions is 20 ~ 40 %. The direct heating of deuterium ions ($\omega = 2\Omega_{CD}$) is quite small (~ 1 %). The rise of deuterium temperature in Fig. 2 will be, therefore, explained in terms of collisional heating. The rf power delivered to each species can be, in principle, deduced from the time derivatives of the plasma parameters at the time of the turn-on/turn-off of the rf pulse ($\dot{n}_e(r), \dot{T}_e(r)$ and $\dot{T}_H(r)$). It is confirmed that the partition of the rf power derived from experimental data is quantitatively in agreement with that estimated with the computer code [16,19].

Energy confinement time

The energy confinement time has been studied for ICRF-heated plasmas. For auxiliary-heated plasmas there are two conceptions of the energy confinement time: i.e., the global energy confinement time defined by $\tau_{E,g} = W_P/P_{input}$, and the incremental one by $\tau_{E,inc} = \partial W_P/\partial P_{aux.}$, where $P_{input} = P_{ohmic} + P_{aux.}$ The present heating power is too low to check the validity of these two scalings, even though the auxiliary heating power by the rf reaches a level about 8 times larger than the ohmic power. Hereafter we discuss only the global energy confinement

time.

Figure 4 shows the global energy confinement time as functions of (a) the total input power $P_{input} = P_{ohmic} + \alpha P_{rf}$, of (b) the plasma current and of (c) the plasma density, respectively. The total stored energy W_P has been derived from the equilibrium vertical field, where the internal inductance l_i is estimated from the measured electron temperature profile. The profile data of plasma parameters ($n_e(r)$,$T_e(r)$ and $T_i(r)$) also give the total stored energy. The stored energy figures derived by these two independent methods are in agreement within an accuracy of 10 %. For the auxiliary heating power P_{aux}, the rf power absorbed by the bulk plasma, αP_{rf}, has been employed. The coupling efficiency α has been derived from the time derivative of the total stored energy at the time of the turn-off of the rf power, i.e., $|\dot{W}_P| = \alpha P_{rf}$. It is observed that the coupling efficiency is unity at the low power level $P_{rf} < 1$ *MW*, and begins to decrease gradually down to 70 % at $P_{rf} = 2$ *MW* [20]. The data in Fig. 4 include the effect on the coupling efficiency, when the rf power is changed.

Figure 4(a) shows the deterioration of the energy confinement time as the rf power is increased. The confinement time predicted by Kaye-Goldston (K-G) L-mode scaling [21] is also presented. We can see that experimental data are quantitatively in good agreement with those of K-G scaling, although the degradation factor of the confinement time, γ, defined by $\tau_{E,g} \propto P_{input}^{-\gamma}$, is slightly smaller (in experimental data $\gamma_{exp} = 0.38$) than that of K-G scaling ($\gamma_{K\text{-}G} = 0.58$). As shown in Fig.4(b), an improvement of the energy confinement time is observed when the plasma current is increased. The dependence on the plasma current is similar to that in K-G scaling. When the density is increased, a remarkable improvement of the energy confinement time has been observed (Fig.4(c)). This is quite different from the prediction of K-G scaling, where $\tau_E \propto \bar{n}_e^{0.26}$. We should remark that, in contrast to experiments done on other tokamak devices, ICRF heating

experiments on the JIPP T-IIU tokamak have been carried out at a density range well below the critical density for Alcator-type saturation of the ohmic phase.

MHD activity

MHD bursts correlated to sawteeth activity are observed on the signal of the magnetic probe. Figure 5 shows the magnetic probe $\dot{B}_\theta$ and soft X-ray signals for I_P=220 kA ($q(a)$ = 4.0) and I_P=280 kA ($q(a)$ = 3.1) at P_{rf} = 2 MW. During the rf pulse, and especially in its later phase, periodic MHD bursts can be seen, and they are coincident with the m=1/n=1 precursor of the sawtooth crash. The mode number of these bursts is confirmed to be m=2/n=1. Similar MHD bursts have usually been observed in high power NBI heating experiments [22,23], where it has been confirmed experimentally and theoretically that this mode (m=2/n=1) is driven by m=1/n=1 internal kink mode through toroidal coupling due to the high-β_P effect, and is mainly localized near the q=1 surface [24].

When the MHD burst begins, the poloidal beta values for the two cases in Fig. 5 are the same (i.e., β_P = 0.5). The threshold rf power for these MHD bursts is $P_{rf} \sim 1.2$ MW and 0.9 MW at I_P = 220 kA and 280 kA, respectively, and the corresponding β_P values are 0.5 for both cases. Therefore, we can conclude that these MHD bursts begin to appear when $\beta_P \geq 0.5$. In the case of I_P = 220 kA the amplitudes of MHD bursts are much smaller and the repetition time is much shorter than in the case of I_P = 280 kA. These characteristics are in agreement with the theoretical prediction, where in the case of high $q(a)$ the field line reconnection at the q=1 surface occurs much more rapidly than in the case of low $q(a)$ because of the increasing shear at the q=1 surface, resulting in small magnetic fluctuations at the plasma surface [24].

We should remark that although these MHD bursts become larger with increases in the plasma current, the energy confinement time becomes longer. Therefore, these MHD bursts do

not influence the energy confinement time. No fishbone-like signals are observed. This is theoretically consistent with the fact that the value of $\beta_T q(a)$ is much smaller in these discharges (i.e., $\beta_T q(a) = 0.017 \sim 0.018$) than the threshold value observed in PLX ($\beta_T q(a) > 0.045$) [25].

IV. Profile consistency for ICRF-heated plasmas

It has been observed that even when the heat deposition profile is widely changed in NBI [26-28] or ECH [29] heating experiments, the electron temperature profile does not change at all and responds only to the safety factor $q(a)$ [26,30], while the density profile is controllable using pellet injection [31]. Theoretically some explanations for this so-called profile consistency have been presented in the framework of the MHD(e.g., tearing mode [32,33] or sawteeth effect [34]) and microturbulence [35] theories. Meanwhile, in TFTR experiments (including the supershot [36] and the current ramp-up [37] experiments), a more restricted profile has been reported, where the electron temperature profile at the outer region of the $q = 1$ surface is independent of even the safety factor, and decouples from the current density profile.

In the above-mentioned experiments, NBI-heated plasmas have mainly been analyzed. It is then very important to examine the validity of the concept of profile consistency for ICRF-heated plasmas, because the heating scheme is quite different. Here we are concerned with the electron temperature profiles for high power ICRF-heated plasmas in the JIPP T-IIU tokamak. The spatial profile and the time evolution of the electron temperature have been measured with a 10-channel grating polychromator for ECE measurement ($\Delta t = 200$ μs and $\Delta r/a \sim 0.17$). The plasma center is determined from the inversion points of the sawteeth, measured on the high- and low-field sides of the plasma center by the ECE system. The shift of the magnetic axis is observed to be $2 \sim 2.5$ cm at

P_{rf} ~ 2 MW, which is in agreement with that estimated with the β_P value.

The electron temperature profile is discussed in terms of the peaking parameter defined by the commonly used form $T_e(0)/\langle T_e \rangle_{vol}$. In Fig. 6 and 7, the peaking parameters are plotted as functions of the rf power and of the safety factor $q(a)$ respectively; the data in the steady-state phase (i.e., $t \sim 180$ ms in Fig. 2) are employed and the variation due to sawteeth activity is also presented. Even when the rf power is changed over a wide range ($0 < P_{rf} < 2$ MW), the peaking parameter is not very sensitive to the rf power at a fixed safety factor, as shown in Fig. 6, although the scatter of the data becomes larger for the high $q(a)$ case. Figure 7 shows the strong dependence of the peaking parameter on the safety factor, and almost all of the data are covered by the following inequality [34];

$$q^{2/3}(a) < T_e(0)/\langle T_e \rangle_{vol} < q(a). \qquad (1)$$

In ICRF heating, it is possible to regulate the deposition profile of the auxiliary heating power without changing the parameters of the main plasmas. Here we have controlled the deposition profile by changing the phase difference $\Delta\varphi$ of neighboring antenna elements shown in Fig. 1, as reported by R. Ando *et al.* [12], in which it has been shown that the deposition profile in electrons is broader for $\Delta\varphi = 0$ than that for $\Delta\varphi = \pi$. In Fig. 8 the peaking parameter is plotted as a function of phase difference, and the deposition profiles are also presented for $\Delta\varphi = 0$ and π. With regard to the data for the steady-state phase, we can say that the peaking parameter is also insensitive to the deposition profile of the rf power. However, it has been observed in the transient phase (i.e., just after the switch-on of the rf pulse, $t \sim 140$ ms in Fig. 2), that the electron temperature profile follows a deposition

profile; that is, the peaked deposition profile ($\Delta\varphi = \pi$) gives rise to a peaked electron temperature profile. Experimental data also show that this peaked profile relaxes to the constraint profile with a time constant of 10 ~ 20 *ms*, which is comparable with the energy confinement time, and is not so rapid as reported in Alcator-C [31] and TFTR [37].

Furthermore, it has been confirmed that the electron temperature is invariant, even when the deposition profile is regulated by changing the toroidal field strength while keeping the fixed H-minority content, with the movement of the mode conversion layer in $\Delta r/a \sim 0.25$.

We conclude from these experiments that in high power ICRF-heated plasmas the electron temperature profile is a function of the safety factor $q(a)$, and is insensitive to the ICRF power and the deposition profile. We should, however, note that the electron temperature profile follows the deposition profile in the transient phase, and takes about 10 ~ 20 *ms* to recover to the constraint profile, (i.e., $\tau_{recover} \sim \tau_E$).

V. Reduction of radiation loss and modelling of impurity suppression for ICRF-heated plasmas

To inject an rf power as high as $P_{rf} = 2$ *MW* without significant degradation of the plasma parameters, it is indispensable to solve problems related to radiation loss and plasma disruption. Here we have solved these problems with (i) a proper conditioning of limiter/wall materials and (ii) gas-puffing synchronized to the rf pulse in combination.

Radiation loss with different limiter/wall conditions

Power loss due to radiation is a major problem in high power ICRF heating experiments. In order to suppress radiation loss, we have examined various materials for the surface of the limiter and the vessel wall. In the first stage of our experiments stainless steel (S.S.) limiters were employed; the

maximum input rf power attained without disruption was below 0.5 *MW*. By replacing the stainless steel limiters with carbon tiles we have achieved the successful suppression of radiation loss in ohmic discharges.

In ICRF experiments, however, the radiation problem has still remained to stand in the way of higher power injection. In repeated experiments at a fixed rf power of 1.3-1.35 *MW*, the radiation power gradually increases from 1.0 to 1.5 *MW* with the number of discharges. This result suggests that the contamination of the carbon tile surface by metal impurities advances with the frequency of discharge. During the rf pulse the stored plasma energy is lost with the decrease of the electron temperature in the central region. From an analysis of the space-resolved bolometric measurement and the spectroscopic one, we have found that metal impurities such as iron are the dominant source of radiation loss around the plasma center due to excitation of their L-shell electrons. Hence, we have tried coating the surface of the limiter/wall with carbon to suppress metal impurity contamination. This technique, so-called carbonization, is described in the following section.

Figure 9 shows the dependence of radiation loss on the input rf power for various conditions of the limiter/wall surface. One can see an obvious suppression of the radiation loss with the improvement of the limiter/wall condition. The carbonization technique has allowed us to achieved rf injection as high as 2 *MW* without significant degradation of the plasma parameters. As a result the radiation loss during the rf pulse is suppressed to 30 ~ 40 % of the total input power, as seen in Figs.2 and 9. In particular, radiation loss at the core region of the plasma is suppressed low enough to be of minor importance for the power balance in the plasma.

Even for plasmas with carbonization, the radiation loss becomes extremely large again at I_P = 150 *kA*, as shown in Fig. 9, while at I_P > 200 *kA* the radiation loss does not depend on the plasma current. We have observed that just after the

switch-on of the rf pulse, the rate of the density increase at I_P = 150 *kA* is about 2 times faster than that at I_P > 200 *kA*. The maximum rf power is, in consequence, limited below 1 *MW* by plasma disruptions due to excessive particle influx. At the position of r/a = 0.5, which corresponds to the cyclotron resonance, the minimum energy E_{min} of the loss cone is 9.6 *keV* for I_P = 150 *kA*, while the value of E_{min} becomes 20.7 *keV* for I_P = 220 *kA*, assuming $j(r) = j(0)(1-(r/a)^2)^3$. The effective tail temperature of hydrogen ions is $T_{eff,H}$ = 4 ~ 7 *keV*. Therefore, the increase in radiation loss at the low plasma current may be attributed to the sputtering induced by high energy ions.

Carbonization

In connection with metal impurity problems the technique of *in situ* carbon coating was first reported by the TEXTOR group [38,39]. A procedure similar to that adopted in TEXTOR was applied to the JIPP T-IIU tokamak [40]. The temperature of the vacuum chamber was 100 °C at highest, and was usually around room temperature. The gas employed was a mixture of 20 % CH_4 and 80 % H_2. A voltage of 400 *V* was applied between the electrode and the chamber, giving an average current density of ~ 2.5 $\mu A/m^2$. Through a glow discharge of a few hours, a carbon layer of thickness 300 ~ 900 Å was formed with a toroidal uniformity within a factor of three. The hydrogen concentration in the layer was estimated from ERDA and TDS to be 40 ~ 50 % in atomic number. We applied an additional glow discharge with D_2 gas for, at least, 4 hours to replace hydrogen with deuterium in the layer, to attain the condition of H/(H+D) ~ 10 % for H-minority heating experiments. Characteristics of the carbon layer thus formed are presented elsewhere [41].

We compare typical discharges at the rf power of 1.2-1.3 *MW* with and without carbonization in Fig. 10. Without carbonization, the radiation power increases monotonically during the rf pulse to be comparable to the input rf power. Spatially resolved bolometric measurement indicates a remarkable

increase in the radiation power around the plasma center. The electron temperature at the plasma center rises for the first 10 *ms* of the rf pulse, but drops below ~ 400 *eV* in the later phase and the stored energy can not be sustained. These result may suggest that some thermal collapse takes place at the plasma center, although it is not crucial for the plasma current to be disrupted.

With regard to plasmas without carbonization, a space-resolved bolometric measurement revealed that the radiation was dominated by that from the central region of the plasma. A calculation of impurity transport shows that iron lines associated with excitation of L-shell electrons dominate the radiation loss within half a minor radius of the plasma column. It was experimentally confirmed that the temporal evolution and the rf power dependence of these line intensities are very similar to those of bolometric radiation. In consequence, it is likely that iron ions with L-shell electrons are the dominant source of radiation loss in the plasma, particularly around the plasma center through a transport inward.

With carbonization, the radiation loss is suppressed to a sufficiently low level. Particularly in the center region, the radiation power is ~ 0.2 MW/m^3, which is about one tenth of that without carbonization. Thus the radiation power is of minor significance to the power balance. Furthermore, no appreciable collapse is observed in the electron temperature at the center during the rf pulse.

The effect of carbonization on each impurity species is inferred from the change in the intensities of prominent lines thereof. To identify the species which were the dominant source of the radiation loss, we observed various VUV lines of carbon, oxygen and iron with and without carbonization. For several prominent lines the intensity ratios in the case of carbonization to that of non-carbonization are plotted in Fig. 11. One can see a drastic change in the power radiated

through the iron lines over a wide range of ionic states. With carbonization the intensities decrease to 1/20 on average. In oxygen lines the intensities also decrease by a factor of 3 ~ 5, while the intensities slightly increase in carbon lines. It is concluded that the radiation loss due to iron impurity, which is dominant in plasmas without carbonization, is drastically reduced with carbonization, resulting in a remarkable reduction in the total radiation loss.

Although the radiation loss is suppressed well by carbonization, another problem arises therefrom: recycling is considerably enhanced by the carbonized wall to be much larger than unity. This causes a density increase up to a limit at which the plasma is terminated by disruption. The TEXTOR group successfully controlled the recycling rate by keeping the wall temperature at 350 °C during carbonization [38]. Since in the JIPP T-IIU tokamak the wall temperature is limited below 100 °C, we have spent about 100 shots with titanium gettering, to make the recycling rate controllable.

Gas puffing and edgy recycling

In high power ICRF experiments we perform gas puffing synchronized to rf pulse to avoid plasma disruption, by increasing plasma density (in addition to the unavoidable density increase due to the rf heating, as shown in Fig. 3). The remarkable increase in the density likely influences the thermal structure, particularly in the outer region of the plasma column. Study on the thermal structure may give a clue for understanding plasma stability and the mechanism of impurity release.

In an attempt to watch the outer plasma region, we observed oxygen lines in VUV wavelengths to deduce the local electron temperature and density [42]. The electron temperature can be derived from the intensity ratio of dipole-transition lines of the same charge state, which follow excitation from the ground state with energies much different from each other. For O IV, V

and VI ions we measured the ratio of 2s-3p transitions to the resonance lines to derive the electron temperature in the environment thereof. For O VII we measured the intensity ratio of 2s-4p to 2p-3d, which has a positive dependence on the electron temperature, although the difference in excitation energies is not sufficient to derive the temperature without taking other processes into account.

Figure 12 shows the time behaviors of the line intensity ratios of O IV - O VII in two cases ((a) without and (b) with carbonization). In Fig. 12(b), the pulse of the gas-puffing is switched on 20 *ms* earlier than the rf pulse, to distinguish the effect of the gas-puffing from that of the rf heating. We can see that the local electron temperatures deduced from O IV - VI rapidly drop in coincidence with the gas-puffing. The region where O IV-VI ions are abundant is about $r/a > 0.8 \sim 0.9$. In contrast, the electron temperature from O VII does not change with the gas-puffing, but begins to increase when the rf pulse is switched on. These characteristics are confirmed by a Thomson scattering measurement. Here we should remark the electron temperature deduced from the line intensity ratio. If the plasma was in local ionization equilibrium at the local electron temperatures, O V and VI would be most abundant at temperatures of 20 ~ 30 *eV*. The fact that local electron temperatures deduced from O IV - VI are much higher than those in local ionization equilibrium, indicates the presence of significant transport toward the core plasma region.

In discharges without carbonization (Fig. 12(a)), the electron temperature in the outer region ($r/a > 0.8 \sim 0.9$) begins to gradually recover during the rf pulse. The spectroscopic data show that emissions from an iron impurity increase in the later phase of the rf pulse, although these are slightly suppressed when the gas-puffing is switched on. These experimental results suggest that the gas-puffing is very effective in suppressing the impurity release from the wall, by reducing the electron temperature in the outer region

$r/a > 0.8 \sim 0.9$. In discharges with carbonization, the electron temperature is kept at the reduced level during the rf pulse (Fig. 12(b)). This may be attributed to the enhanced recycling caused by the carbonized wall, which behaves just like an effective gas-puffing during the rf pulse. Of course, the major contribution to the suppression of the total radiation loss comes from replacing or covering the limiter/wall with low-Z materials, as described in the previous sections.

Another role of the gas-puffing is to control the plasma disruption. Regarding the amount of the gas-puffing, there exists a narrow window. Excessive or insufficient gas-puffing brings the plasma to disruption. This window is also strongly sensitive to the limiter/wall condition. As confirmed experimentally in Fig. 12, the gas-puffing makes the electron temperature lower at the outer plasma region. The mechanism to avoid the disruption will be, then, explained by the tailoring of the current density profile in the outer region [43].

VI. Conclusions

In the JIPP T-IIU tokamak, high power ICRF heating experiments have been conducted up to an extremely high power density ($\sim 2\ MW/m^3$) with a total rf power of $P_{rf} = 2\ MW$. Principal results are summarized as follows.

(a) With the injection of $P_{rf} = 2\ MW$, electron and ion temperatures of $T_e(0) = 2\ keV$ and $T_D(0) = 1.7\ keV$ have been achieved at the density of $\bar{n}_e = 7 \times 10^{19}\ m^{-3}$. The percentage of the rf power delivered to electrons is about 60 ~ 80 %, and the remainder is delivered to hydrogen ions, resulting in a high energy tail. The deuterium ions are heated through collisions.

(b) The global energy confinement time reveals characteristics similar to Kaye-Goldston L-mode scaling based on NBI-heated plasmas, although the density dependence is stronger in experimental data ($\tau_E \propto \bar{n}_e^{0.6}$) than that in K-G scaling

($\tau_{E,K\text{-}G} \propto \overline{n}_e^{0.26}$).

(c) When the β_P value is larger than $\beta_P = 0.5$, m=2/n=1 MHD bursts have been observed in coincidence with the m=1/n=1 precursor of the sawtooth crash. These MHD bursts do not, however, influence the energy confinement time.

(d) The electron temperature profile has been intensively examined, by changing the rf power, the safety factor and the power deposition profile. It is found that the peaking parameter $T_e(0)/\langle T_e \rangle_{vol}$ of the electron temperature profile strongly depends on the safety factor, but is insensitive to other parameters, although during the transient phase ($t < \tau_E$) the electron temperature profile follows the deposition profile.

(e) The radiation loss problem has been intensively studied. We have concluded that the most effective method of reducing the total radiation loss is to replace or to cover as much of the metallic surface (i.e., limiter, antenna and wall) as possible, with a low-Z material (e.g., carbon tile or carbonization). Gas-puffing has been applied, being synchronized to the rf pulse. It has been found from spectroscopic measurement that the electron temperature in the outer region of the plasma column ($r/a > 0.8 \sim 0.9$) is suppressed by the gas-puffing, resulting in the reduction of the impurity release due to sputtering. Moreover, an adequate amount of the gas-puffing is very helpful in tailoring the current density profile in the outer region in order to avoid plasma disruption.

Acknowledgements

The authors would like to thank Dr. A. Fukuyama and Prof. T. Amano for their theoretical support, and express their appreciation to Prof. Y. Sakamoto and his colleagues for supervising the carbonization. The authors would also like to thank Dr. T. Kato for her fruitful comments on VUV data.

(a) Present address: National Laboratory for High Energy Physics, Oho, Tsukuba, Ibaraki 305, Japan

References

[1] Hosea, J., Bernabei, S., Colestock, P., Davis, S.L., Efthimion, P., et al., Phys. Rev. Lett., 43 (1979) 1802.

[2] Hwang, D.Q., Hosea, J., Thompson, H., Wilson, J.R., Davis, S., et al., Phys. Rev. Lett., 51 (1983) 1865.

[3] Hosea, J., Bell, R., Bitter, A., Cavallo, A., Cohen, S., *et al.*, in Controlled Fusion and Plasma Heating (Proc. 12th Europ. Conf., Budapest, 1985), Vol.9F Part II, European Physical Society (1985) 120.

[4] Watari, T., Ohkubo, K., Akiyama, R., Ando, R., Eckhartt, D., et al., in Plasma Physics and Controlled Nuclear Fusion Research 1986 (Proc. 11th Int. Conf., Baltimore, 1986) Vol.I, IAEA, Vienna (1987) 495.

[5] Odajima, K., Funahashi, A., Hoshino, K., Kasai, S., Kawakami, T., et al., ibid., 151.

[6] Steinmetz, K., Söldner, F.X., Eckhartt, D., Janeschitz, G., Leuterer, F., et al., ibid., 461.

[7] Vandenplas, P.E., Delvigne, T., Descamps, P., Durodie, F., Jadoul, M., et al., ibid., 485.

[8] JET Team, ibid., 449.

[9] JT-60 Team, in Plasma Physics and Controlled Nuclear Fusion Research 1986 (Proc. 11th Int. Conf., Kyoto, 1986) Vol.I, IAEA, Vienna (1987) 11.

[10] Schmidt, J., Bateman, G., Bushnell, C., Citrolo, J., Colestock, P., *et al.*, ibid., 259.

[11] Coppi, B., Comments Plasma Phys. Controll. Fusion, 5, (1980) 261.

[12] Ando, R., Sato, K., Watari, T., Ogawa, Y., Kawahata, K., *et al.*, Nucl. Fusion, 28 (1988) 147.

[13] Kawahata, K., Sakai, K., Ando, R., Ohara, S., Fujita, J., Jpn. J. Appl. Phys., 27, (1988) 2349.

[14] Morita, S., Ogawa, Y., Watari, T., Akiyama, R., Kadota, K., Kawasumi, Y., Ozaki, T., Sasao, M., Sato, K., in Controlled Fusion and Plasma Heating (Proc. 14th Europ. Conf. ,

Madrid, 1987), Vol.III, European Physical Society (1987) 874.

[15] Ogawa, I., Kawahata, K., Ogawa, Y., Watari, T., Noda, N., Masai, K., Kako, E., Tanahashi, S., Toi, K., Fujita, J., J. Phys. Soc. of Japan, 56, (1987) 535.

[16] Ozaki, T., Kadota, K., Ogawa, Y., Fujita, J., Rev. Sci. Instrum., 59(8) (1988) 1503.

[17] Stix, T.H., Nucl. Fusion, 15, (1975) 737.

[18] Fukuyama, A., Nishiyama, S., Itoh, K., Itoh, S.-I., Nucl. Fusion, 23 (1983) 1005.

[19] Ogawa, Y., Akiyama, R., Ando, R., Hamada, Y., Hirokura, S., *et al.*, in Controlled Fusion and Plasma Heating (Proc. 13th Europ. Conf. , Schliersee, 1986), Vol.II, European Physical Society (1986) 25.

[20] Ida, K., Ogawa, Y., Toi, K., Kawahata, K., Watari, T., *et al.*, Power Absorption and Confinement Studies of ICRF-Heated Plasma in JIPP T-IIU Tokamak, Nagoya Univ., Inst. of Plasma Physics, Rep. IPPJ-886 (1988).

[21] Kaye, S.M. and Goldston, R.J., Nucl. Fusion, 25 (1985) 65.

[22] Yamamoto, S., Maeno, M., Suzuki, N., Azumi, M., Tokuda, S., *et al.*, Nucl. Fusion, 21, (1981) 993.

[23] Dunlap, J.L., Carreras, B.A., Pare', V.K., Holmes, J.A., Bates, S.C., Bell, J.D., Hicks, H.R., Lynch, V.E. and Navarro, A.P., Phys. Rev. Lett., 48, (1982) 538.

[24] Holmes, J.A., Carreras, B.A., Hicks, H.R., Lynch, V.E. and Rothe, K.E., Phys. Fluids, 25, (1982) 800.

[25] McGuire, K., Goldston, R., Bell, M., Bitter, M., Bol, K., *et al.*, Phys. Rev. Lett., 50, (1983) 891.

[26] Wagner, F., Gruber, O., Lackner, K., Murmann, H.D., Speth, E., *et al.*, Phys. Rev. Lett., 56 (1986) 2187.

[27] Murmann, H., Wagner, F., Becker, G., Bosch, H.S., Brocken, H., *et al.*, in Controlled Fusion and Plasma Heating (Proc. 13th Europ. Conf., Schliersee, 1986), Vol.I, European Physical Society (1986) 216.

[28] Goldston, R.J., Fredrickson, E., McGuire, K., Zarnstorff,

M., Bell, M., *et al.*, ibid., 41.

[29] Alikaev, V.V., Bagdasarov, A.A., Berozovskii, E.L., Berlizov, A.B., Borshegovskii, A.A., *et al.*, ibid., 111.

[30] Taylor, G., Efthimion, P.C., Arunasalam, V., Goldston, R.J., Grek, B., Hill, K.W., Johnson, D.W., McGuire, K., Ramsey, A.T. and Stauffer, F.J., Nucl. Fusion, 26 (1986) 339.

[31] Greenwald, M., Gwinn, D., Milora, S., Parker, J., Parker, R., *et al.*, Phys. Rev. Lett., 53 (1984) 352.

[32] Furth, H.P., Plasma Physics and Controlled Fusion, 28 (1986) 1305.

[33] Ohyabu, N., Lee, J.K., deGrassie, J.S., Nucl. Fusion, 23 (1986) 593.

[34] Waltz, R.E., Wong, S.K., Greene, J.M., Dominguez, R.R., Nucl. Fusion, 26 (1986) 1729.

[35] Coppi, B., Tang, W., Electron Energy Transport and Magnetic Curvature Driven Modes, Rep. PPPL-2151, Princeton Plasma Physics Laboratory, Princeton, NJ (1984).

[36] Goldston, R.J., Arunasalam, V., Bell, M.G., Bitter, M., Blanchard, W.R., *et al.*, in Plasma Physics and Controlled Nuclear Fusion Research 1986 (Proc. 11th Int. Conf., Kyoto, 1986) Vol.I IAEA, Vienna (1987) 75.

[37] Fredrickson, E.D., McGuire, K.M., Goldston, R.J., Bell, M.G., Grek, B., Johnson, D.W., Morris, A.W., Stauffer, F.J., Taylor, G., Zarnstorff, M.C., Nucl. Fusion, 27 (1987) 1897.

[38] Winter, J., J. Nucl. Materials, 145-147, (1987) 131.

[39] Winter, J., Waelbroeck, F., Wienhold, P., Esser, H.G., Könen, L., Braun, Emmoth, B., Sätherblom, H.E., J. Nucl. Materials, 128&129, (1984) 841.

[40] Noda, N., Ogawa, Y., Masai, K., Ogawa, I., Ando, R., *et al.*, Jpn. J. Appl. Phys., 25, (1986) L397.

[41] Noda, N., Hori, Y., Masai, K., Ogawa, Y., Hirokura, S., *et al.*, J. Nucl. Materials, 145-147, (1987) 709.

[42] Kato, T., Masai, K., Mizuno, J., J. Phys. Soc. of Japan,

52, (1983) 3019.

[43] Toi, K., Itoh, S., Kadota, K., Kawahata, K., Noda, N., Sakurai, K., Sato, K., Tanahashi, S., Yasue, S., Nucl. Fusion, 19, (1979) 1643.

Figure Captions

Fig. 1 Experimental arrangement of the JIPP T-IIU tokamak. ICRF antennas installed at the high-field side, the carbon limiters and typical diagnostics are presented.

Fig. 2 Typical discharge of $P_{rf} \sim 2$ *MW*; the plasma current I_P, the one-turn voltage V_{loop}, the line-averaged density $\bar{n}_e$, the total radiation power P_{rad}, the central electron/deuterium temperatures $T_{e,D}(0)$, measured by ECE and FNA, respectively, the total stored energy W_P(total) derived from the equilibrium vertical field and the stored energy density of electrons $W_e(0)$ derived from kinetic data.

Fig. 3 Central electron/ion temperatures $T_{e,i}(0)$ and the line-averaged density $\bar{n}_e$ as a function of the rf power. The data at the steady-state ($t \sim 180$ *ms* in Fig. 2) are plotted. Since the electron temperature has a peak at the early phase of the rf pulse ($t \sim 140$ *ms*), peak values of the electron temperature are also presented. Ion temperatures are measured with four different diagnostic tools; (A) a charge-exchange fast neutral analyzer (FNA) of E//B mass-separation type, (B) a crystal spectrometer (*TiXXI* w 2.61Å), (C) charge-exchange recombination spectroscopy (CXRS) with *CVI* 5292Å and (D) VUV spectrometer (*FeXXII* 845.5Å). The power of NBI for CXRS is less than 0.2 *MW*.

Fig. 4 Global energy confinement times τ_E defined by $\tau_E = W_P/P_{input}$ as functions of (a) the total input power $P_{input} = P_{ohmic} + \alpha P_{rf}$, of (b) the plasma current I_P and of (c) the line-averaged density $\bar{n}_e$, respectively. The confinement time predicted by Kaye-Goldston L-mode scaling [21] is also presented.

Fig. 5 Magnetic probe $\dot{B}_\theta$ and soft X-ray signals for (a)

I_P = 220 kA($q(a)$ = 4.0) and (b) I_P = 280 kA($q(a)$ = 3.1). MHD bursts (m=2/n=1 mode) correlated to sawteeth activity are observed on the signal of the magnetic probe.

Fig. 6 Peaking parameter of the electron temperature profile defined by $T_e(0)/\langle T_e\rangle_{vol}$ as a function of the rf power for two cases ($q(a)$ = 2.7 and 3.8).

Fig. 7 Peaking parameter $T_e(0)/\langle T_e\rangle_{vol}$ as a function of the safety factor $q(a)$, including the data in the range of $0 < P_{rf} < 2$ MW. The variation of $T_e(0)/\langle T_e\rangle_{vol}$ due to the sawteeth activity is also shown, and at $q(a) > 5$ there is no sawteeth. Almost all data are bounded by the inequality of $q^{2/3}(a) < T_e(0)/\langle T_e\rangle_{vol} < q(a)$, as pointed out by R. Waltz, *et al*. [34].

Fig. 8 Peaking parameter $T_e(0)/\langle T_e\rangle_{vol}$ as a function of the phase difference, $\Delta\varphi$, of neighboring antenna elements in two different time; one is just after the switch-on of the rf pulse, called the "transient phase" (i.e., $t \sim 140$ ms in Fig. 3), and another is the steady-state phase (i.e., $t \sim 180$ ms). In the cases of $\Delta\varphi = 0$ and π, the power deposition profiles [12] are presented.

Fig. 9 Total radiation loss as a function of the rf power for various wall/limiter conditions; (i) the stainless steel limiter, (ii) the carbon limiter without carbonization, and (iii) the carbon limiter with carbonization. The plasma current is larger than 200 kA for all cases, except data denoted by "A", where I_P = 150 kA. As shown with an arrow, in repeated experiments at a fixed rf power of 1.3-1.35 MW, the radiation power gradually increases from 1.0 to 1.5 MW with the number of discharges.

Fig. 10 Discharge characteristics (a) without and (b) with

carbonization for P_{rf} = 1.2-1.3 MW, where the total radiation loss P_{rad}, the central electron temperature $T_e(r=0)$ measured by ECE and Thomson scattering, the total stored energy W_P and the radiation loss profile $E(r)$ measured by a 12-ch. bolometer array.

Fig. 11 Intensity ratio in the case of carbonization to that of non-carbonization; I(with carbonization)/I(without one). Various VUV lines for iron, oxygen and carbon are compared. *) read as FeXXIV 192 Å line.

Fig. 12 Time behaviours of line intensity ratios of O IV - O VII measured with a VUV spectrometer for two different cases ((a) without and (b) with carbonization). For signals of O IV - VI, the electron temperatures in the environments of these ions are deduced and presented, where we should note that the vertical scale is not linear to the electron temperature. It is not straightforward to deduce the electron temperature for O VII, while the intensity ratio has a positive dependence on the electron temperature.

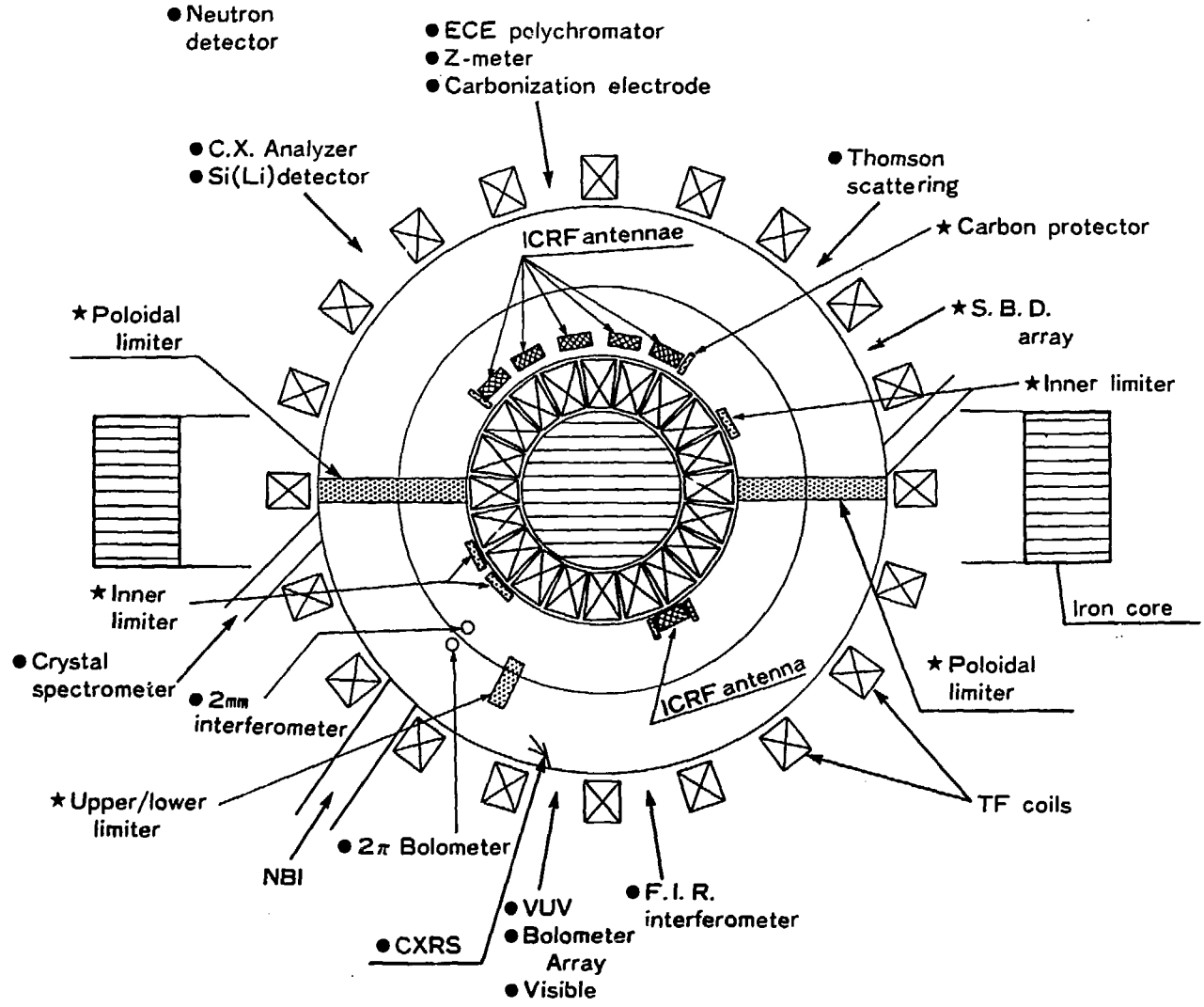
● Neutron detector
● ECE polychromator
● Z-meter
● Carbonization electrode
● C.X. Analyzer
● Si(Li)detector
● Thomson scattering
★ Carbon protector
ICRF antennae
★ Poloidal limiter
★ S. B. D. array
★ Inner limiter
Iron core
★ Inner limiter
● Crystal spectrometer
● 2mm interferometer
ICRF antenna
★ Poloidal limiter
★ Upper/lower limiter
TF coils
NBI
● 2π Bolometer
● VUV
● Bolometer Array
● Visible
● CXRS
● F. I. R. interferometer

Fig. 1

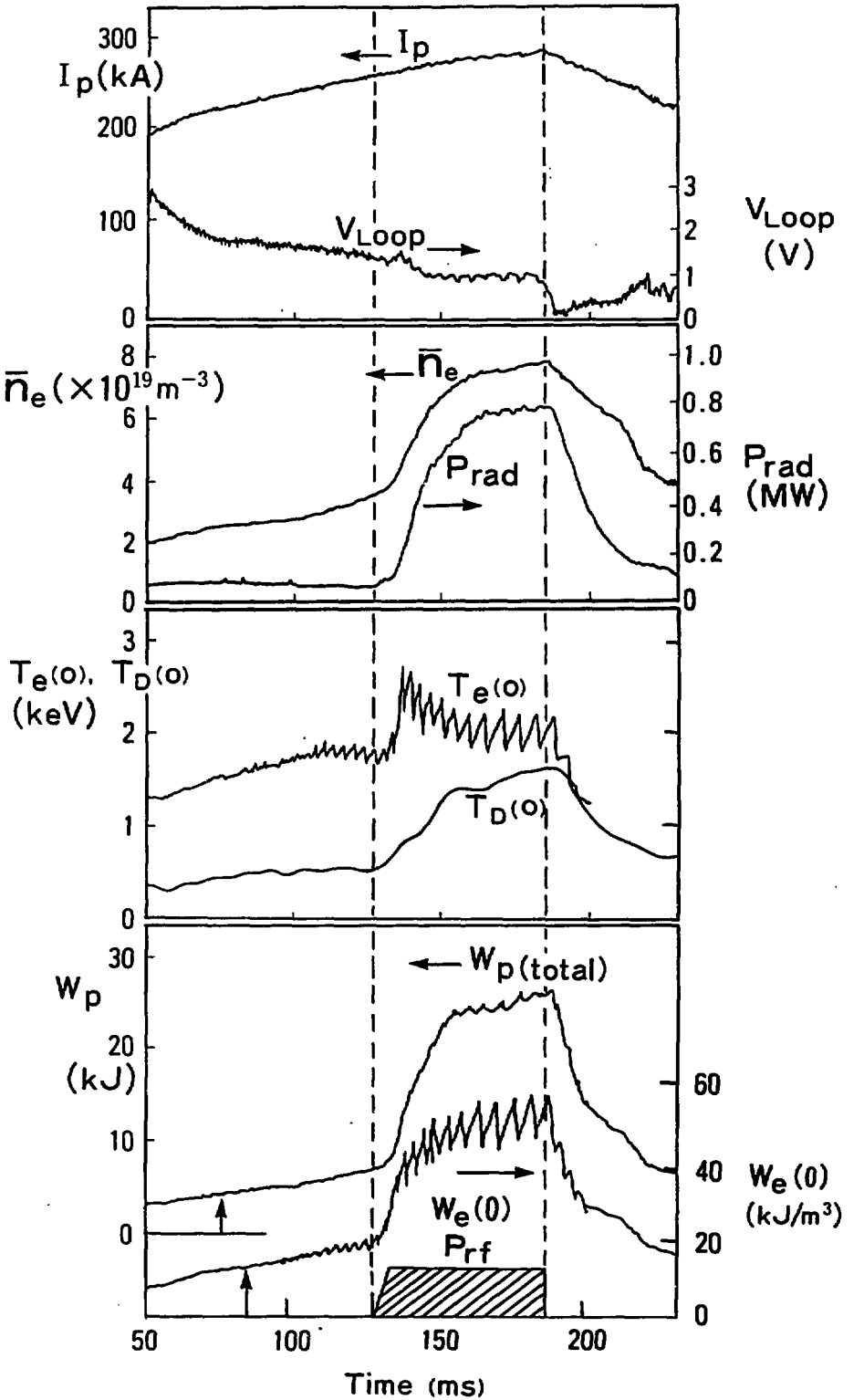
300
I_p(kA)
200
100
0
I_p
V_{Loop}
3
2
1
0
V_{Loop}
(V)
8
$\bar{n}_e$($\times 10^{19}$m^{-3})
6
4
2
0
$\bar{n}_e$
P_{rad}
1.0
0.8
0.6
0.4
0.2
0
P_{rad}
(MW)
3
T_e(o), T_D(o)
(keV)
2
1
0
T_e(o)
T_D(o)
30
W_p
20
(kJ)
10
0
W_p(total)
W_e(0)
P_{rf}
60
40
20
0
W_e(0)
(kJ/m^3)
50
100
150
200
Time (ms)

Fig. 2

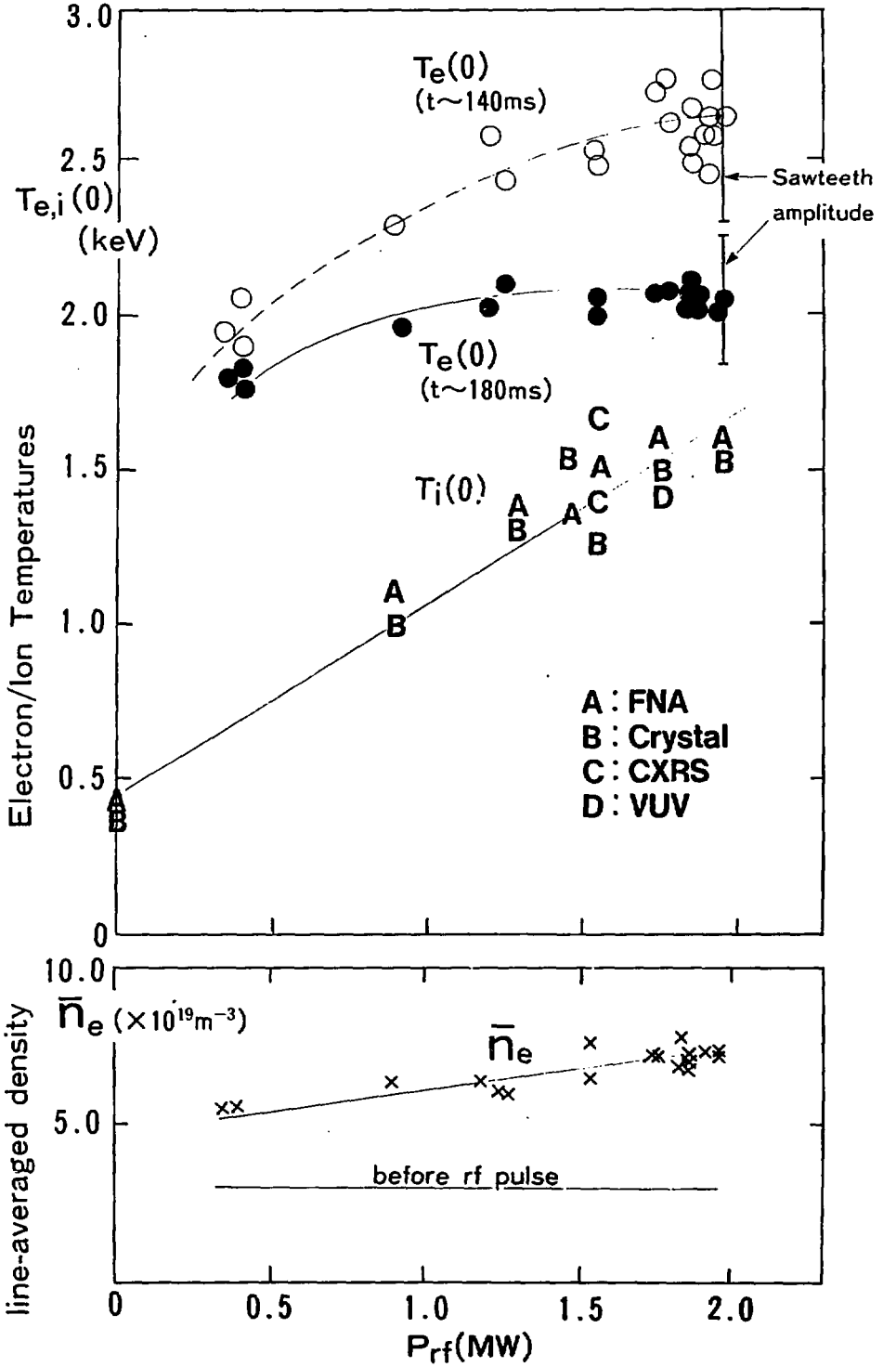
3.0
2.5
2.0
1.5
1.0
0.5
0
Te,i (0)
(keV)
Te(0)
(t~140ms)
Te(0)
(t~180ms)
Ti(0)
Sawteeth
amplitude
Electron/Ion Temperatures
A : FNA
B : Crystal
C : CXRS
D : VUV
10.0
5.0
line-averaged density
n̄e (×10^19m^-3)
n̄e
before rf pulse
0
0.5
1.0
1.5
2.0
Prf(MW)

Fig. 3

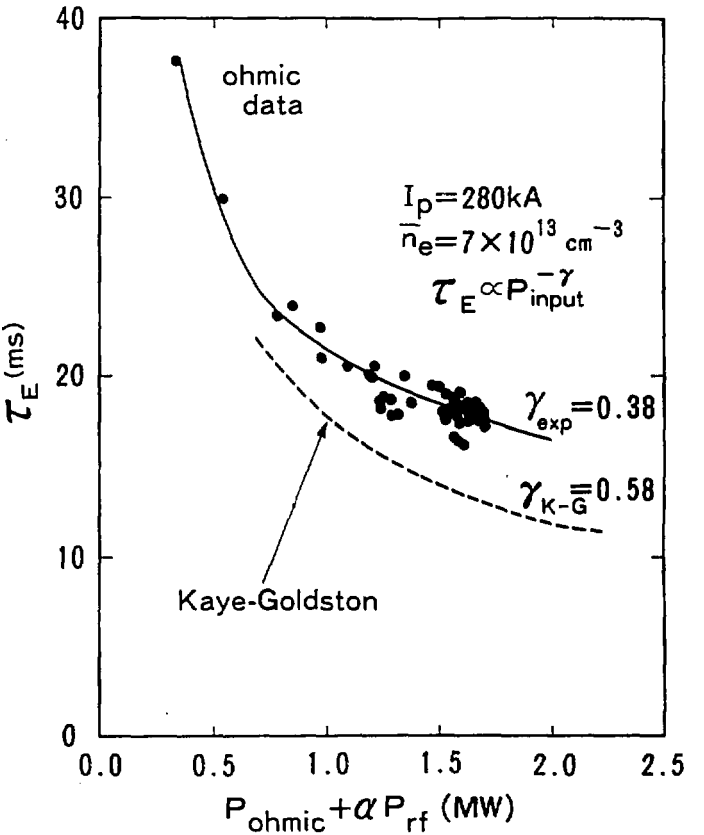
40
30
20
10
0
0.0
0.5
1.0
1.5
2.0
2.5
ohmic
data
I_p=280kA
$\bar{n}_e=7\times10^{13}$ cm^{-3}
$\tau_E \propto P_{input}^{-\gamma}$
γ_{exp}=0.38
$\gamma_{K\text{-}G}$=0.58
Kaye-Goldston
τ_E (ms)
$P_{ohmic}+\alpha P_{rf}$ (MW)

Fig.4(a)

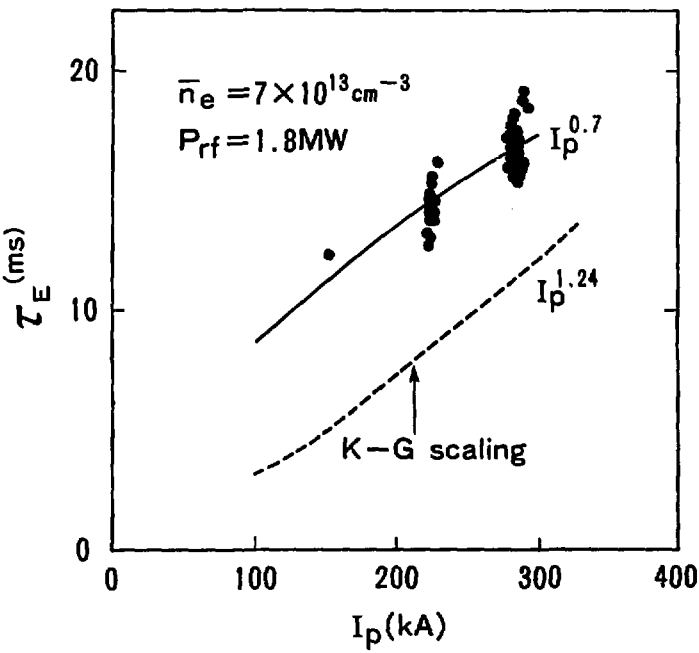
20
10
0
$\bar{n}_e = 7 \times 10^{13} cm^{-3}$
$P_{rf} = 1.8 MW$
$I_p^{0.7}$
$I_p^{1.24}$
K−G scaling
τ_E (ms)
0
100
200
300
400
I_p(kA)

Fig.4(b)

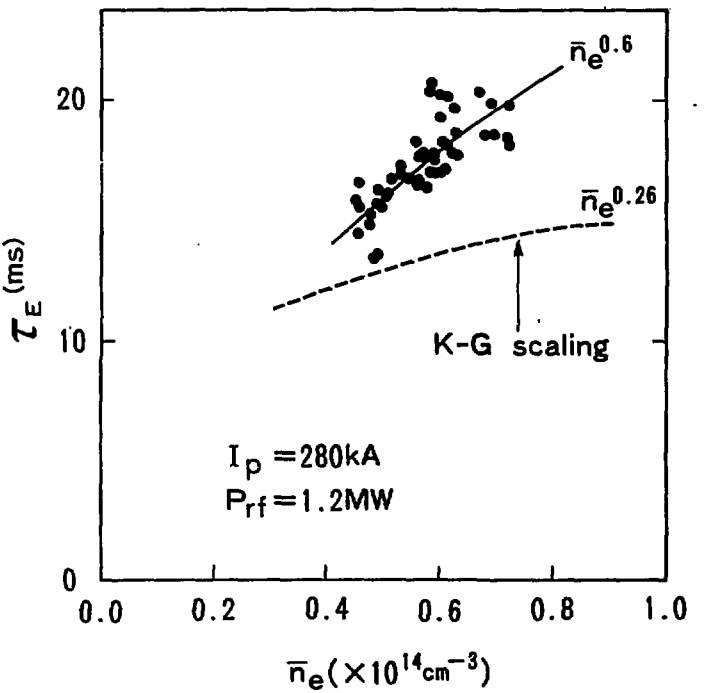
$\bar{n}_e^{0.6}$
$\bar{n}_e^{0.26}$
K-G scaling
I_p =280kA
P_{rf}=1.2MW
τ_E (ms)
20
10
0
0.0
0.2
0.4
0.6
0.8
1.0
$\bar{n}_e(\times 10^{14}cm^{-3})$

Fig.4(c)

Fig.5

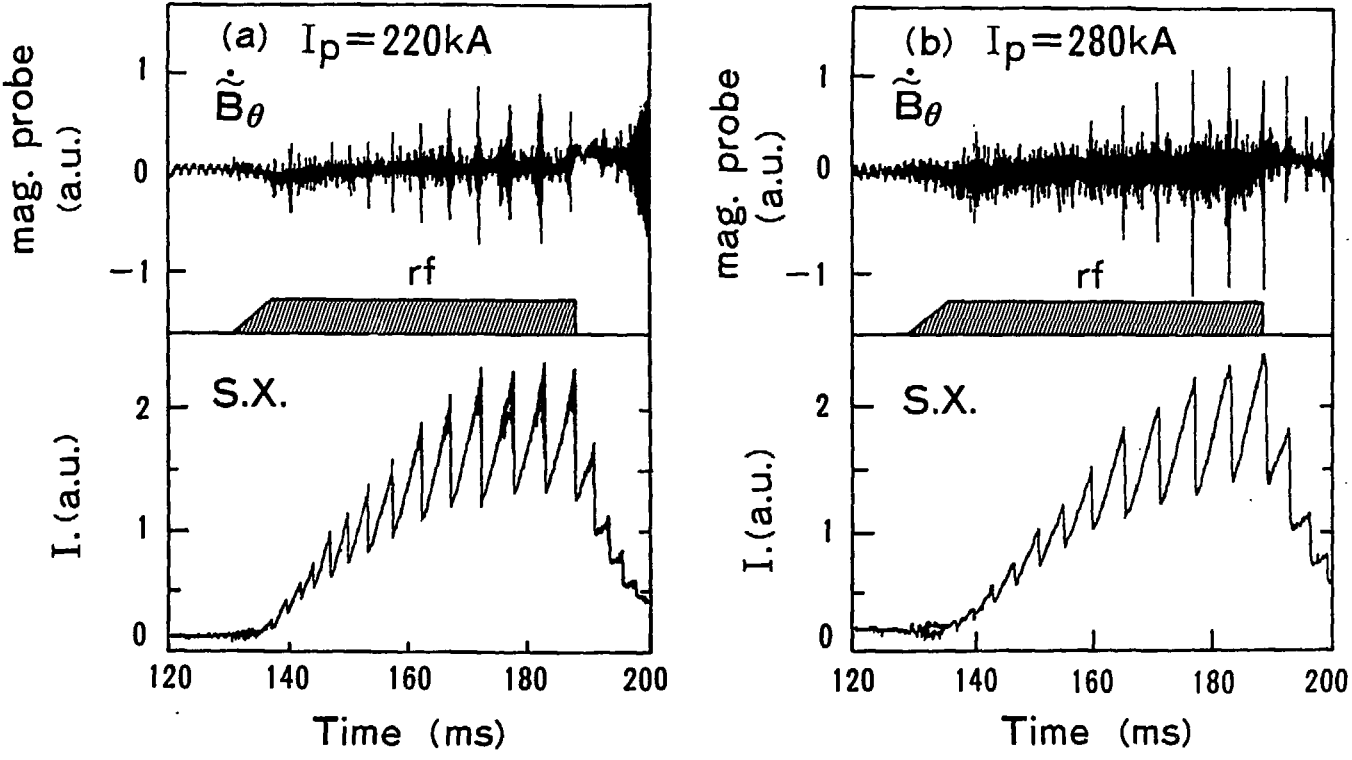
(a) I_p=220kA
$\dot{\tilde{B}}_\theta$
mag. probe (a.u.)
rf
S.X.
I.(a.u.)
Time (ms)
(b) I_p=280kA
$\dot{\tilde{B}}_\theta$
mag. probe (a.u.)
rf
S.X.
I.(a.u.)
Time (ms)

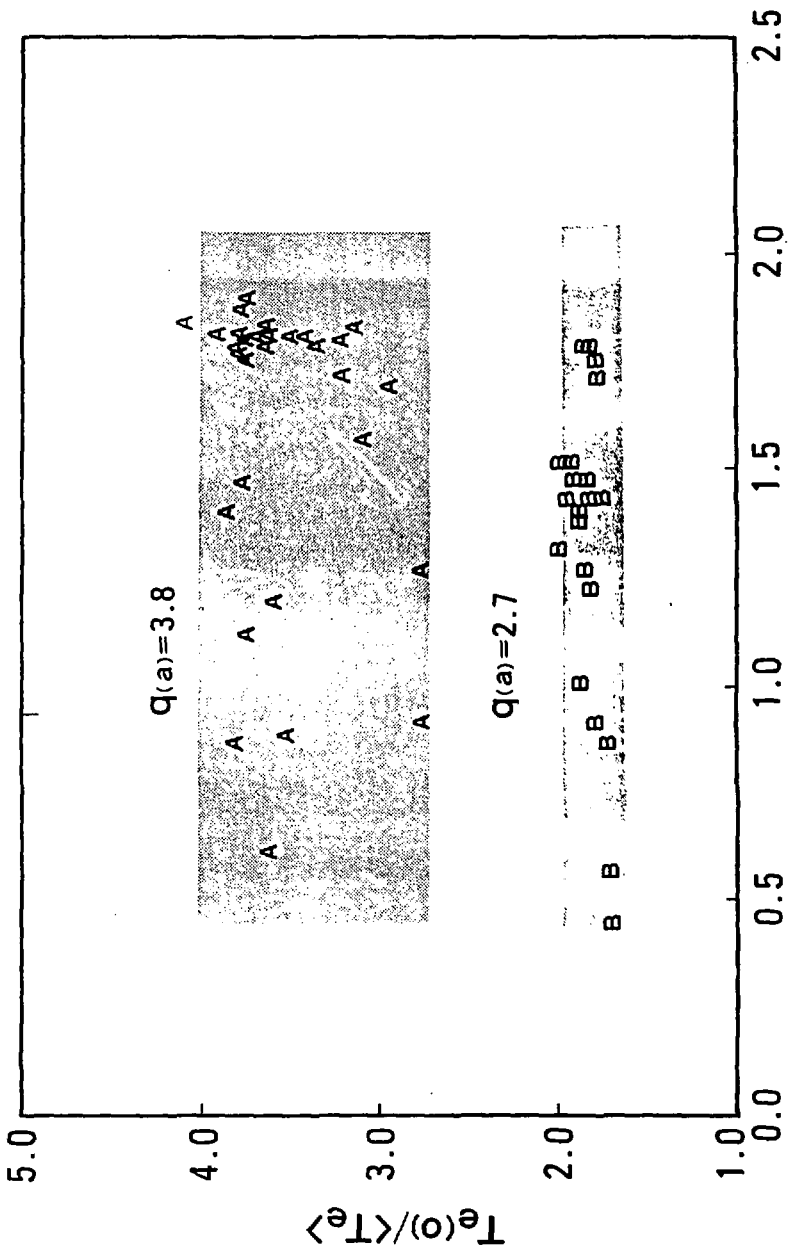
5.0
4.0
3.0
2.0
1.0
0.0
0.5
1.0
1.5
2.0
2.5
$T_e(o)/\langle T_e \rangle$
P_{rf}(MW)
$q_{(a)}$=3.8
$q_{(a)}$=2.7
A
B

Fig.6

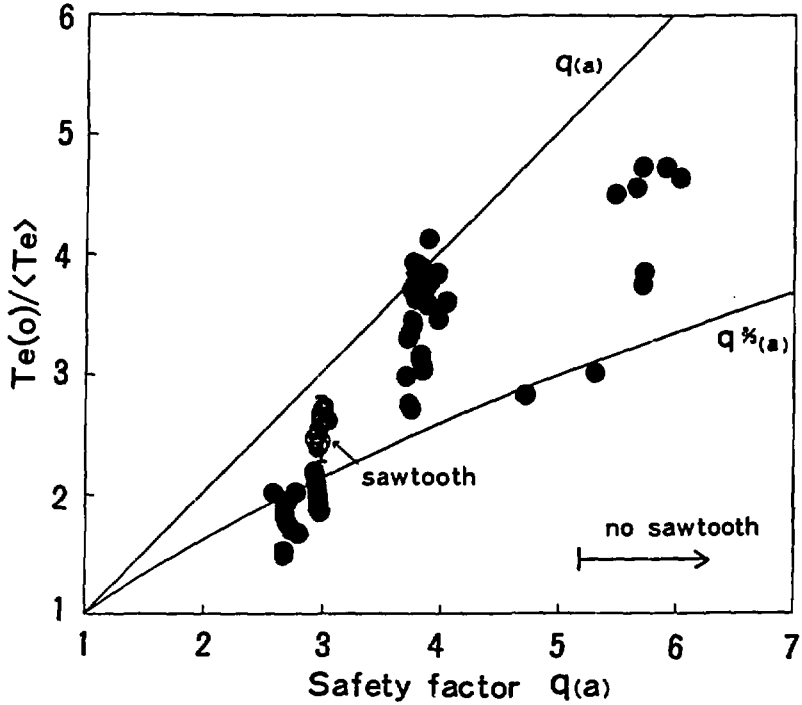
6
5
4
3
2
1
Te(o)/<Te>
q(a)
q ⅘(a)
sawtooth
no sawtooth
1
2
3
4
5
6
7
Safety factor q(a)

Fig.7

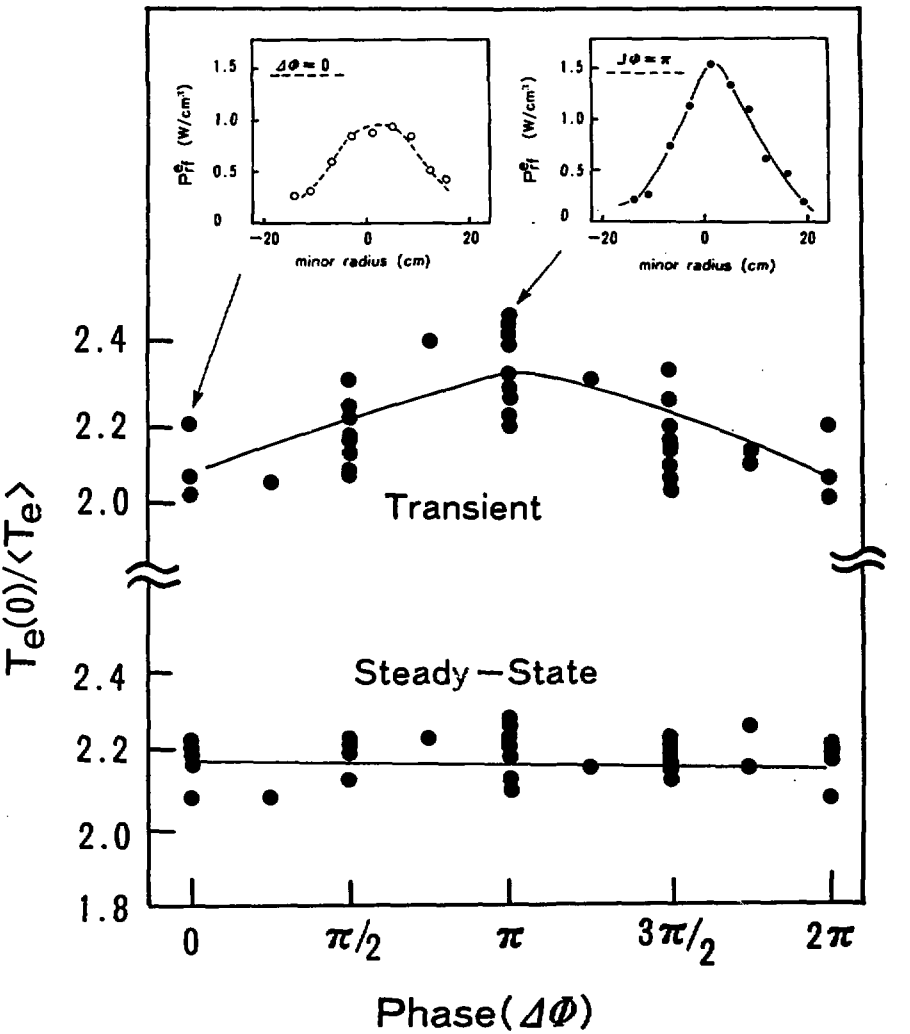
ΔΦ≈0
ΔΦ≈π
1.5
1.0
0.5
0
−20
0
20
minor radius (cm)
2.4
2.2
2.0
1.8
Transient
Steady−State
Te(0)/<Te>
0
π/2
π
3π/2
2π
Phase(ΔΦ)

Fig. 8

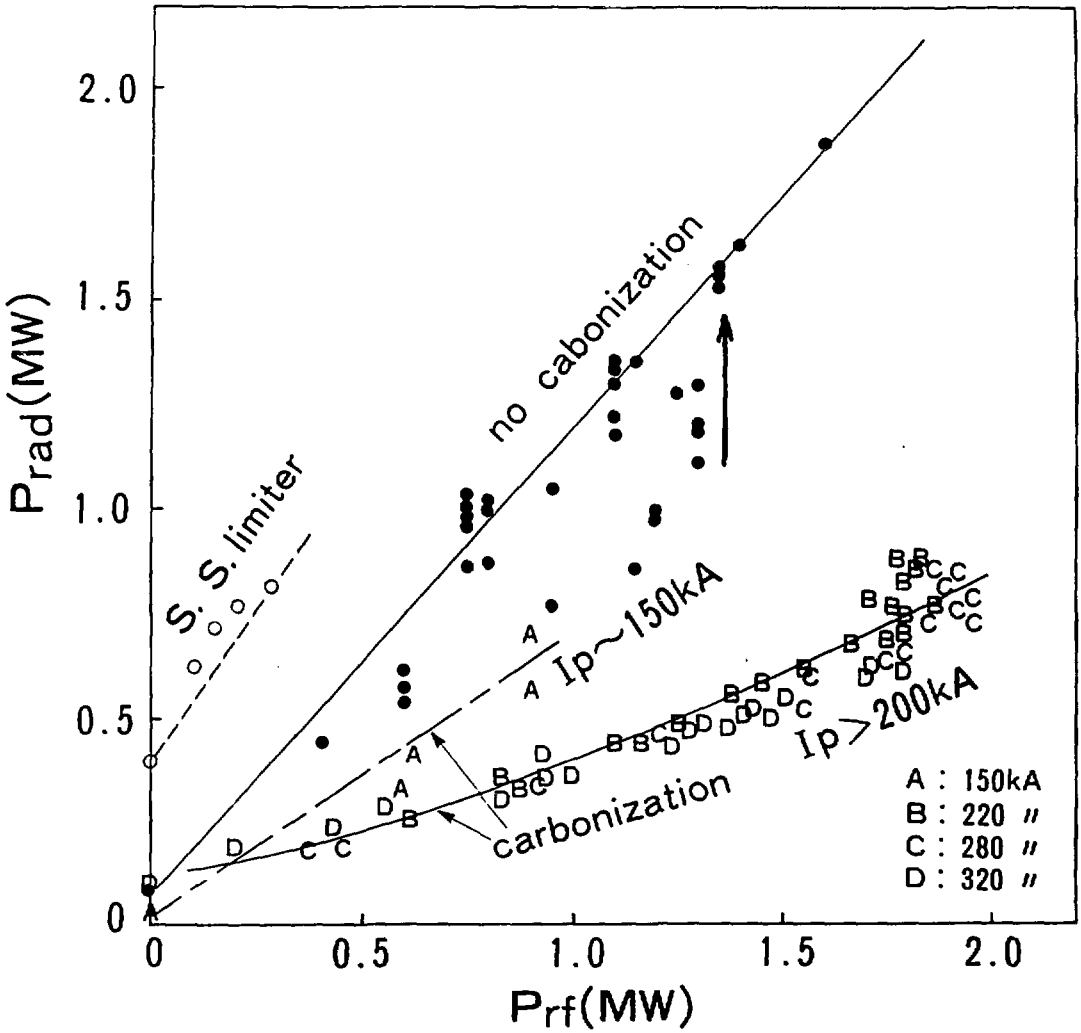
2.0
1.5
1.0
0.5
0
0
0.5
1.0
1.5
2.0
Prad(MW)
Prf(MW)
S. S. limiter
no cabonization
Ip~150kA
Ip>200kA
carbonization
A : 150kA
B : 220 //
C : 280 //
D : 320 //

Fig.9

(a)without carbonization (b) with carbonization

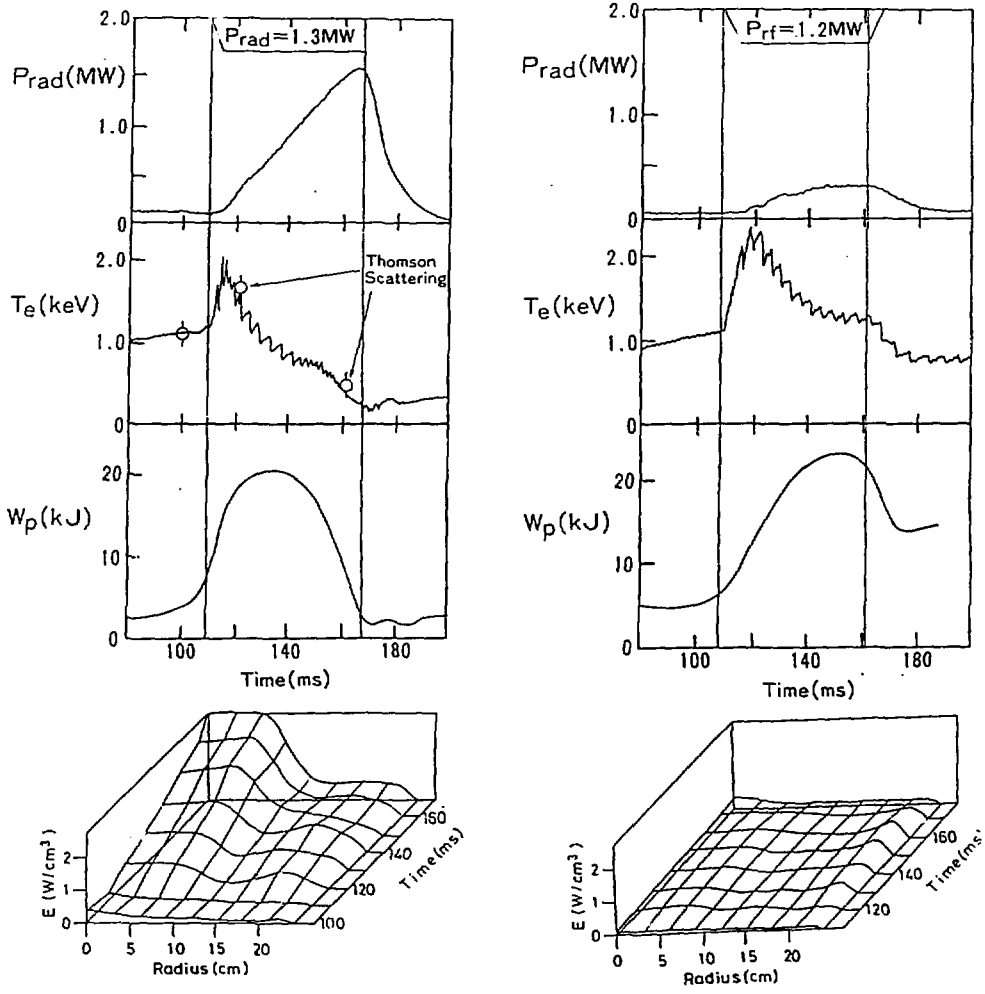

Fig.10

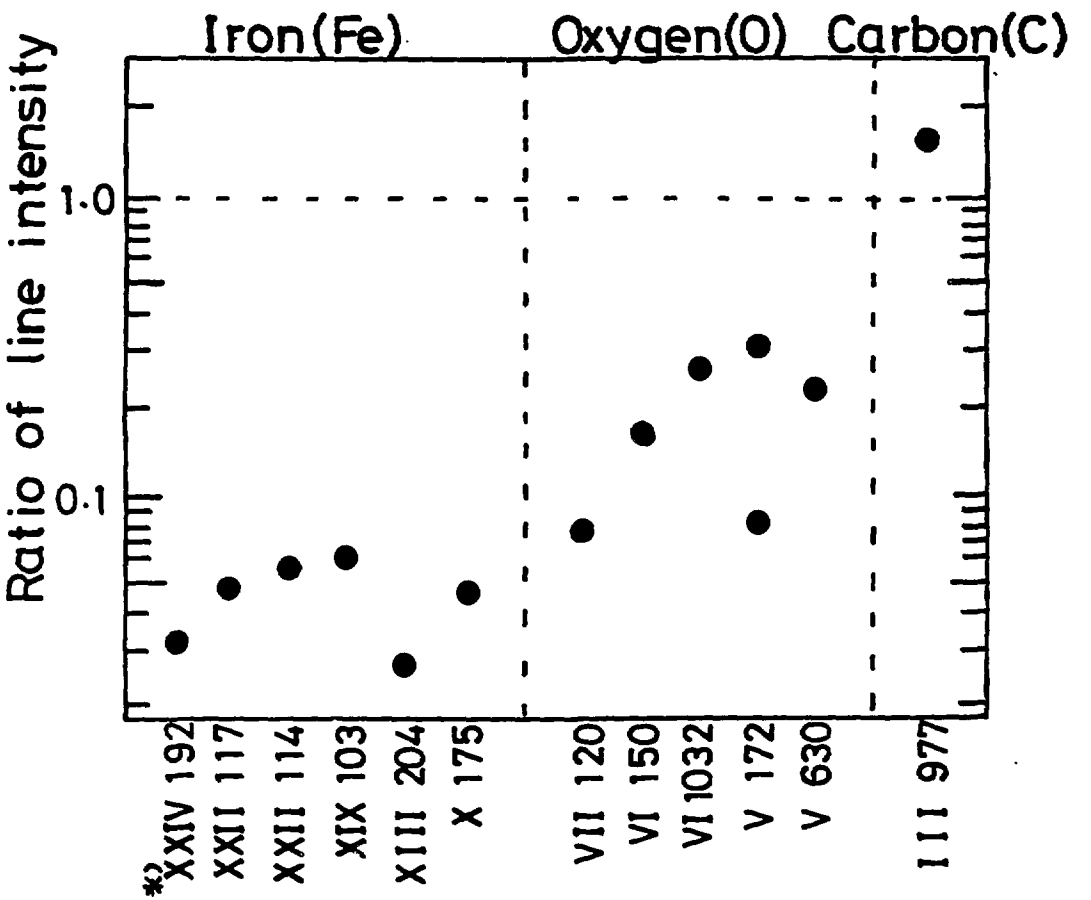
Iron(Fe)
Oxygen(O)
Carbon(C)
Ratio of line intensity
1·0
0·1
*2 XXIV 192
XXII 117
XXII 114
XIX 103
XIII 204
X 175
VII 120
VI 150
VI 1032
V 172
V 630
I I I 977

Fig.11

Fig.12

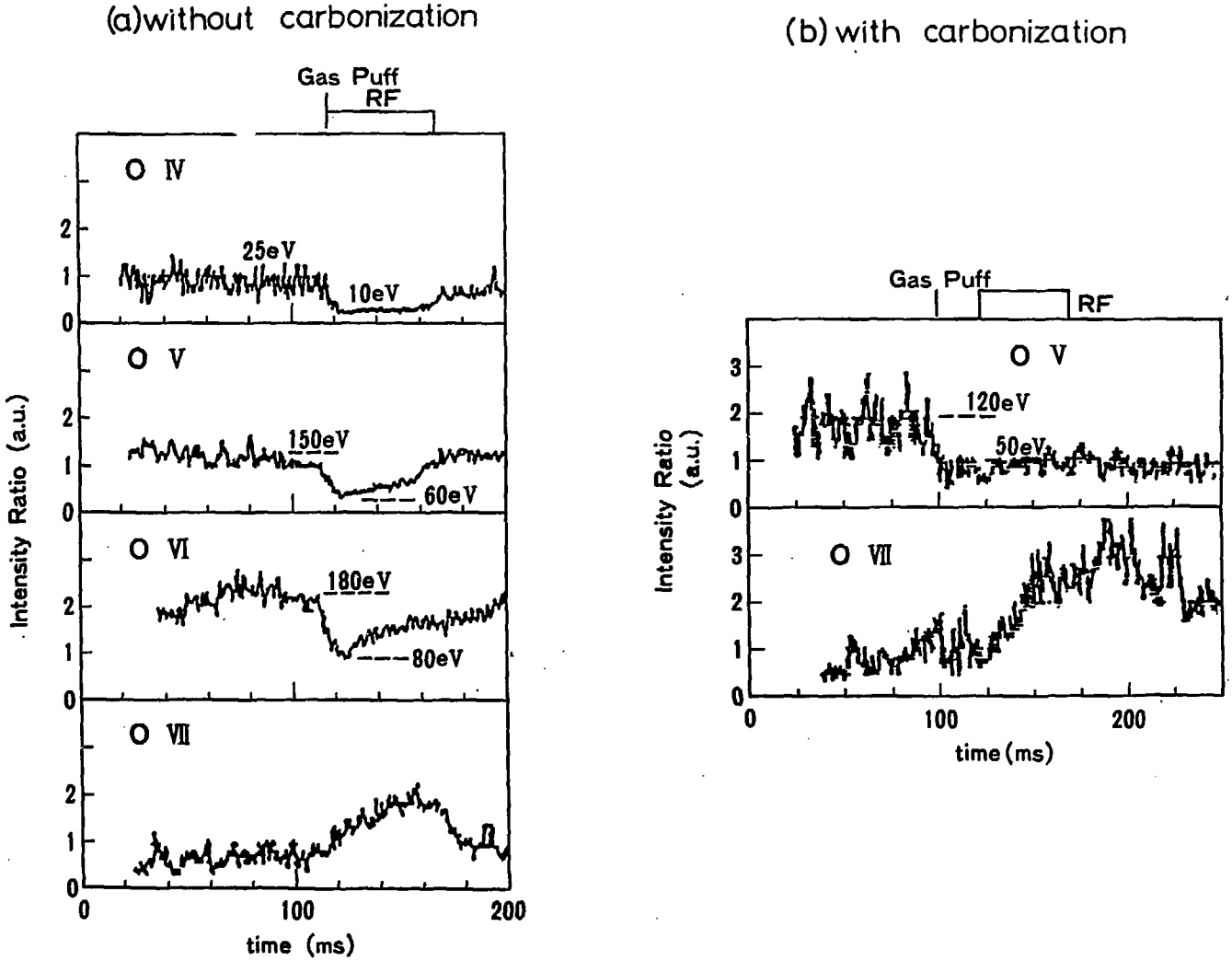
(a)without carbonization
Gas Puff
RF
O IV
25eV
10eV
O V
150eV
60eV
O VI
180eV
80eV
O VII
Intensity Ratio (a.u.)
time (ms)
(b) with carbonization
Gas Puff
RF
O V
120eV
50eV
O VII
Intensity Ratio (a.u.)
time (ms)